

**Particle-Image-Velocimetry Measurements in Organic Liquid Multiphase
Systems for an Optimal Reactor Design and Operation**

Katharina Zähringer^{1*}, Lisa-Maria Wagner¹, Dominique Thévenin¹, Patrick Siegmund³,

Kai Sundmacher^{2,3}

1: Lehrstuhl für Strömungsmechanik und Strömungstechnik, Otto-von-Guericke-Universität Magdeburg, Germany

2: LSVT, Otto-von-Guericke-Universität Magdeburg, Germany

3: Max Planck Institute for Dynamics of Complex Technical Systems, Magdeburg, Germany

* Corresponding author: katharina.zaehringer@ovgu.de

ABSTRACT

Abstract:

Hydrodynamic features are very important to find an optimal reactor design for the hydroformylation of long-chain alkenes. For this purpose, and for the validation of theoretical reactor concepts, velocity measurements in a model reactor system are necessary. Due to the difficult reaction conditions found in reality (toxic thermomorphic organic solvent system, high pressure, high temperature, limited fields of view in typically used model reactors) such measurements are not an easy task. In this work, comparative Particle-Image-Velocimetry (PIV) measurements have been used *to find out if 1) the substitution of the solvent with water, and 2) reducing operation pressure* still lead to similar results. For this purpose, PIV measurements have been performed in a stirred tank reactor under reaction conditions (organic solvents, high pressure, high temperature), but also with water at reduced pressure levels. It is found that pressure (as expected), and also the employed solvents do not have a significant influence on the observed flow structures, although density and viscosity are rather different. Therefore, further systematic experiments are now carried out in a model reactor, completely built out of glass, with water filling, and at atmospheric pressure. A complete hydrodynamic characterization is thus possible, opening the door for optimization of the resulting hydrodynamic field and for detailed comparisons with theoretical reactor design as well as numerical predictions.

Keywords: Hydroformylation, particle-image-velocimetry, reactor design, hydrodynamics, multi-phase system

1. Introduction

On the way towards a generic, model-based design for multi-phase chemical reactors, a continuous reactor allowing the hydroformylation of 1-dodecen to tridecanal has been retained as relevant application example (Kaiser et al. 2016; Kämper et al. 2016; Zagajewski et al. 2014; Zagajewski et al. 2016). To optimize the corresponding process, the hydrodynamic features of this reactor are particularly important and must be characterized in detail, if necessary in the real geometry and under real operating conditions. Dead zones have to be avoided and the re-dosing positions for consumed educts and gasses (Syngas) have to be optimized in order to maximize reaction yield (Hentschel et al. 2015). To support this process, in-situ flow field measurements are needed. Since probe-based measurements impact the hydrodynamic features, non-intrusive optical measurements shall be preferred whenever possible. In order to obtain information concerning velocity fields, Laser-Doppler Anemometry (LDA) and Particle-Image-Velocimetry (PIV) are mostly employed. PIV has been retained for this project, since it delivers information for a macroscopic field of view, and not only at a single point, as is the case for LDA.

There are uncountable publications describing Particle-Image-Velocimetry (PIV) measurements. Most consider aerodynamic applications, but many PIV measurements have been documented for chemical engineering applications

involving a liquid bulk phase in stirred tank reactors; for instance in (Deen et al. 2002; Kim et al. 2001; Pan et al. 2008; Sharp and Adrian 2001; Yoon et al. 2005), to analyze the velocity field near Rushton turbines under different conditions; or in (Baldi and Yianneskis 2003; Kilander and Rasmuson 2005; Sharp et al. 1999; Sheng et al. 2000; Sheng et al. 1998; Sudiyo et al. 2003), where turbulence features have been analysed in stirred tank reactors and used in particular to validate numerical modelling approaches (Sheng et al. 1998; Yoon et al. 2001). The impact of a secondary gas flow on hydrodynamics has been considered, e.g., in (Deen and Hjertager 2002; Hall et al. 2005; Montante et al. 2013).

Still, the continuous liquid phase used in all these studies is almost always water, sometimes glycerol-water mixtures. To the knowledge of the authors, no hydrodynamic study based on PIV measurements in organic solvent systems has been published yet.

Additionally, most published works relying on PIV to characterize hydrodynamic features of chemical reactors have taken place under atmospheric pressure and ambient temperature. Therefore, the connection between such mostly academic PIV studies and real process engineering applications is sometimes not straightforward.

In the present case, a thermomorphic organic solvent system (TMS) is used (figure 1). Depending on its temperature, the mixture can be in a two-phase state (left column of figure 1) or in a single-phase state (right column of figure 1). Such a system is extremely useful in practice, since it delivers excellent conditions both for 1) chemical reactions in a single-phase liquid, followed by 2) an easy separation of the catalyst-

solution from the product in the two-phase state, simply by switching between two different temperature values (Dreimann et al. 2016; McBride et al. 2016). Unfortunately, the hydrodynamic behaviour of such complex solvent systems has not been characterized up to now.

Figure 1

The chemicals used in the real process are organic solvents and toxic. Furthermore, the system has to be heated up to approx. 90°C to attain the single-phase state, and the reactor has only limited optical access due to safety issues, because the reaction also needs high pressure (20 bar) for high yield and selectivity. Therefore, a step-by-step procedure as shown in figure 2 has been retained to check the influence of solvent and pressure on the PIV-measurements. Based on the findings, measurements in a simplified configuration, e.g., a completely transparent model reactor, at atmospheric pressure, might become possible. In the same manner, measurements in water instead of organic solvents might deliver a proper approximation. Both, combined with refraction-index matching, would allow for a far more detailed level of accuracy and would thus deliver more information.

Therefore, in this study, PIV measurements in the original TMS-system at atmospheric and high pressure are compared to measurements in water at different pressure levels. From these results, all further experiments used to validate the theoretical models developed separately (Kaiser et al. 2016) will be planned.

Figure 2 Measurement strategy

2. Experimental setup

The employed experimental setup is shown in figure 3. The experiments were carried out in a stirred tank steel reactor (1, in Fig. 3 top) purchased from Büchi AG with two glass windows (10mm thick), arranged in a 90° angle (see Fig. 3 centre and bottom). The reactor has no baffles, a volume of 1000 ml, an inner diameter of 102mm and a height of 108mm. The diameter of the windows is 40mm and they are located in the vertical centre of the reactor. A 3-blade propeller stirrer ($d=50\text{mm}$) was used for the measurements at two rotational speeds, 200rpm and 400rpm. These rotational speeds always lead to turbulent conditions with maximum Reynolds-Numbers

of 16 600 for water and 31 600 for the TMS systems, with n the

$$Re = n \times d^2 \times \rho / \mu$$

number of revolutions of the stirrer, d the stirrer diameter and ρ and μ the density and viscosity of the fluid respectively. Due to the much lower viscosity, the TMS has about twice the Reynolds number of the water system. But, all examined regimes are already in the fully-developed turbulent regime, leading for stirred systems to constant characteristics, regarding power consumption, mixing times etc. (Zlokarnik 2001). This means, that the flow is mainly dominated by convective inertial effects and not by viscous forces for all configurations considered. The shaft of the stirrer

can be seen through the window, as shown in figure 1 (bottom, right). The stirrer speed has been chosen according to the experimental constraints: first, considering the reaction, which needs sufficient mixing; second, taking into account laser and camera acquisition frequency; third, due to the funnel that is formed at about 600rpm in a way to cover the area of interest, so that no further PIV measurements were possible.

The different liquids (water and TMS-systems) were filled into the reactor and fluorescent tracer particles (FluoOrange, $\lambda_{fl} = 584\text{nm}$) with a mean diameter of $9.84\ \mu\text{m}$, made of melamin resin ($\rho = 1510\ \text{kg/m}^3$, resistant to the solvents), purchased at Microparticles GmbH, were added. The relaxation time of these particles, calculated

as $\tau_p = d_p^2 \rho_p / 18 \times \mu$, has a value of $2.1 \cdot 10^{-5}\ \text{s}$ for the TMS and $8.4 \cdot 10^{-6}\ \text{s}$ for water.

Stokes numbers ($St = \tau_p / \tau_F$) for the tank scale with $\tau_F = d_{\text{stirrer}} / u$, calculated for the

highest measured velocity ($0.3\ \text{m/s}$), have values of $1.3 \cdot 10^{-4}$ for TMS and $5.3 \cdot 10^{-5}$ for

water. Calculated with the Kolmogorov time scale $\tau_K = d_{\text{stirrer}} / (u \times \sqrt{Re})$ Stokes

numbers still are very small with $St = 6.5 \cdot 10^{-3}$ for water and $St = 2.2 \cdot 10^{-2}$ for TMS. This

means that these tracer particles can well follow the flow, even though their density

is rather high. Nitrogen was used to increase the pressure via a tube. Both, pressure

and temperature were continuously controlled and monitored via a Siemens

Miniplant Controlling system. Pressure is given in the following as gauge pressure (overpressure).

Illumination for PIV was provided by a pulsed, frequency-doubled (532nm) Nd-YAG laser (Litron LDY 300, number 3, in Fig. 3 top) with an energy of 54 mJ/P, formed to a 0.5mm thick light sheet (5, in Fig. 3 top) and passed vertically, directly in front of the stirrer axis (Fig. 3 bottom). The time delay between two pulses was 600 μ s. Thus, between two laser pulses, the particles maximally moved by about 180 μ m. Given the thickness of the laser sheet (500 μ m), out-of-plane motion was therefore not a noticeable problem. A LaVision Imager Intense CCD-camera (2) with a 1376x1040 pixel² chip (pixel size: 6.45 μ m x 6.45 μ m), a 105 mm AF Micro Nikkor Nikon lens ($f\#=4$) and a 537 nm long-pass filter, to exclude laser light and reflections, recorded the double PIV-images at an acquisition frequency of 3 Hz. The resulting image resolution was, depending to the first decimal place on the x - or y -direction, around 42 μ m/pix. This means that structures of about 100 μ m and larger can be resolved. The geometrical calibration has been done with a calibration target, mounted on the stirrer shaft, just at the position where the light sheet passes in the reactor. Post-treatment of the images has been done with LaVision Davis 8.4 Software. A multi-pass PIV evaluation was used, with decreasing interrogation area size from 32x32 pixels to 16x16 pixels with 50% overlap and, in the mean, about 5 particles per smallest interrogation area. This resulted in a final vector spacing of 340 μ m. As preprocessing, a time series filter and constant background value subtraction were applied for enhancement of particle contrast in the images, as well as masking of the

window and gas tube. Post-treatment of the obtained vector fields comprised peak ratio filtering and a median filter compared with neighbouring vectors. Then, the obtained 500 individual snapshot vector fields were averaged to a mean vector field, the standard deviation is a measure for velocity fluctuations. The measurements uncertainty has been evaluated using the method of (Wieneke 2015). This method estimates the error induced by the calculation of the displacement field, based on the intensity pattern of the images. It leads to a maximum error of 0.008 m/s for the velocity magnitude, which is about one order of magnitude smaller than the measured velocity differences between Water and TMS. Thus, it can be concluded, that the measured differences are not due to measurement accuracy, but to a real difference.

First, measurements in water at room temperature were performed. Then, the pressure was increased stepwise ($\Delta p=1\text{bar}$) up to 10bar and the flow field was recorded. The same procedure was repeated with two different compositions of the TMS system. The first mixture (TMS 1) consisted of 42 wt% dimethylformamide (DMF), 42wt% decane and 16wt% 1-dodecene and was measured at 94°C. The second mixture (TMS 2) consisted of 32wt% DMF, 48wt% decane and 20wt% 1-dodecene and was measured at 82°C. Both temperatures were just a bit higher than the critical temperature for phase change of the respective system. Liquid density of the TMS-systems at reaction temperature has a value of $\approx 760\text{ kg/m}^3$, while the viscosity, compared to water, is rather small, with 0.4 mPa·s. These properties and compositions are summarized in table 1 together with the employed experimental

conditions. All of the examined parameter combinations show the same qualitative tendencies. Therefore, only a typical case in the mid-pressure range at 5bar with a rotating speed of 400rpm has been chosen exemplarily for the further presentation of the results.

Table 1 Liquid compositions and properties

	DM F wt %	deca ne wt%	dodece ce wt%	wat er wt%	densi ty kg/m ³	dyna mic viscosi ty mPa s	gauge pressu re bar	stirr er spee d rpm	Re -
Wat er	-	-	-	100	1000	1	0-10	200, 400	830 0 166 00
TMS 1	42	42	16	-	760	0.4	0-10	200, 400	158 00 316 00
TMS 2	32	48	20	-	760	0.4	0-10	200, 400	158 00 316 00

Figure 3 Experimental setup

3. Results

3.1 Influence of solvents

To determine the influence of the different solvents, the planar velocity fields of the two TMS mixtures and of water, all at 5 bar and 400rpm stirrer speed, are compared in figures 4, top to Fig. 6. Arrows show the planar 2D-velocity direction, background

colour indicates the corresponding velocity component. The TMS systems are in the single-phase state for the measurements and water is at room temperature. Velocities are averaged over 500 snapshots.

Figure 4 Averaged velocity magnitude (top) and standard deviation of magnitude (bottom) in different solvents at 5bar and 400rpm in m/s.

The highest velocity magnitude is found for all three solvent systems in the area directly in front of the stirrer (centre of the window). To the left side, it decreases homogeneously. On the right side, the gas tube and the temperature probe inside the reactor (masked out, white bar on all following figures), strongly influence the local flow structure. The velocity magnitude there is slightly higher than on the left side. Due to the installed equipment, no symmetry exists in the flow within the vessel.

The corresponding rms-values, representing the flow fluctuations, are also represented in figure 4, bottom. They show the same pattern for all three solvents, but fluctuations are slightly smaller in the case of water. The largest fluctuations are always found at the top of the observation window. This might be caused indirectly by the waves and the funnel at the liquid surface, which is situated about 2cm above the window. The fluctuations on the right side can be explained by the temperature and gas probes that are situated on that side.

Looking at figure 5, which shows the vertical velocity component v_y , a similar situation can be recognized. The highest velocity in y-direction exists directly in front

of the stirrer. The lowest y -velocities are situated on the right side of the vessel, where the probes are installed.

Figure 5 Vertical velocity component v_y in different solvents at 5bar and 400rpm in m/s.

Figure 6 Horizontal velocity component v_x in different solvents at 5bar and 400rpm in m/s.

The horizontal component v_x , shown in figure 6, clearly depicts the rotating fluid motion induced by the stirrer, rotating from the right to the left. Fluid is transported from the right to the left, with the highest horizontal motion in negative coordinate direction. On both sides of the vessel the horizontal component is nearly zero, since fluid comes from the third dimension into the measuring plane.

Regarding absolute velocity profiles, as presented for the centre of the window at $y=20\text{mm}$ in figure 7 (right column), the differences between the solvent systems and water are small. All three fluids show similar velocity profiles.

Figure 7 Relative mean velocity differences between water and TMS solvent systems in % at 5bar and 400rpm. Left: TMS1; centre: TMS2; right: absolute velocity profiles in the centre of the window at $y=20\text{mm}$. Top: mean velocity magnitude; centre: mean vertical velocity component; bottom: mean horizontal velocity component.

Due to the colour scale used in figures 4-6 for clarity, the difference between the mean velocity fields of water and TMS may seem rather strong at first. But, calculating the difference with the mean water results and normalizing it by the mean water velocities, the situation becomes different (figure 7, left and centre column). The deviation is maximum in a small region at the top of the stirrer shaft, with values attaining locally up to 40% for the velocity magnitude (upper row). The funnel, induced by the stirrer, might explain this relatively strong local deviation.

For the vertical and horizontal velocity components (figure 7, centre and lower row), the situation is similar. The deviations reach locally values up to 70% near the stirrer shaft; however, in most positions the relative deviation within the observation window is rather small, with values around 10%. Visible differences between water and the solvent systems are found mainly in the top centre region, close to the stirrer funnel and on the right, next to the gas tube and temperature probe.

The differences between TMS and water are also represented in terms of root-mean-square errors (*RMSE*) in figure 8, thus taking into account the velocity fluctuations.

The *RMSE* is calculated here as:

$$RMSE = \sqrt{\sum (v_i - w_i)^2 / n}$$

, where v_i and w_i are the snap-shot velocity fields of TMS and water respectively and n is the number of snap-shots. This figure shows again that the main differences exist near the stirrer shaft, on top of the viewing window near the liquid surface and on the right side, near the probes. In the central and lower part of the tank, the differences are very small for all

velocity components (Fig. 8), although the bulk liquid densities differ from ≈ 760 kg/m³ (TMS-Systems at reaction temperature) to 998 kg/m³ (water, 20°C), while the viscosity varies from 0.4 mPas (TMS-Systems at reaction temperature) to 1 mPas (water, 20°C)

Figure 8 Root-mean square difference between TMS solvent systems and water of velocity magnitude (top), vertical velocity component (centre) and horizontal component (bottom) in m/s at 5 bar and 400 rpm. Left: TMS1; right: TMS2.

3.2 Influence of pressure

Theoretically, pressure should not have any influence on the hydrodynamics in the reactor. But, since the reaction including gas addition works only under high pressure levels (10-20bars), it still seemed worthwhile to test also this parameter. To check its possible influence, velocity fields at pressures from 0 to 10 bar gauge pressure were acquired for water and for the TMS systems.

Figure 9 shows the averaged velocity magnitude in water at 0 and 9bar gauge pressure and 400rpm. The relative difference attains, as shown in figure 9 (bottom, left), values of maximum 15% near the stirrer shaft. Here, the velocities in water at 0 bar served as a reference and the difference to the 9 bar results has been normalized in this manner. Once more, the *RSME* is calculated for this case (Fig. 9, bottom, right) and the main differences between the 9 bar and 0 bar case are situated near the liquid surface on top of the window and around the temperature probe.

Figure 9 Averaged velocity magnitude [m/s] in water for 0 and 9 bar at 400rpm (top) and relative mean deviation in % (bottom, left) and RMSE difference (bottom, right).

The same procedure was repeated for the first TMS system with similar results, as shown in figure 10. The pressure influence is comparable, with local maxima of 15%. In this case the deviation is calculated with the TMS1 velocities at 0 bar as a reference. The *RMSE* (Fig. 10, bottom, right) has the same aspect as for water. Only at the left border of the window the values seem to be higher. This might be caused by some reflections, visible on the raw images of the 9 bar case.

Figure 10 Averaged velocity magnitude [m/s] in TMS1 for 0 and 9 bar at 400rpm (top) and relative mean deviation in % (bottom, left) and RMSE difference (bottom, right).

In figure 11, the mean velocity magnitudes for the whole pressure range are shown as radial profiles at the window centre position ($y=20\text{mm}$). All curves fall together and no systematic change, related to pressure, can be observed. This confirms that pressure has very little influence on hydrodynamics in this system.

Figure 11 Averaged velocity magnitude profiles (m/s) in TMS1 at 400rpm for different pressure in the centre position of the window ($y=20\text{mm}$).

As a consequence of both investigations, and looking back at figure 2, it is finally possible to work systematically with water as solvent and under atmospheric pressure. This fact tremendously facilitates the full hydrodynamic characterization of the process. Still, local differences near the stirrer shaft and the probes must be kept in mind, even if they do not impact noticeably average properties.

4. Conclusions

PIV-measurements have been carried out in a high-pressure, organic solvent reactor under real reaction conditions, compared to a simple water filling at various pressure levels. These experiments demonstrate that pressure shows no significant influence (as expected), but also that the employed solvent system does not impact noticeably the hydrodynamics in the stirred tank reactor for the range of Reynolds numbers considered. Therefore, further experiments for the validation of theoretical reactor models can be carried out in a model reactor, completely built out of glass, with water filling, and at atmospheric pressure. Such conditions immensely reduce the complexity of experimental studies, and allow accurate measurements of all relevant quantities, opening the door for a deeper understanding of the underlying processes and for validation of companion computations. A complete hydrodynamic characterization is possible in this manner, so that optimal operating conditions can be derived.

Acknowledgements

This work is part of the Collaborative Research Center/Transregio 63 “Integrated Chemical Processes in Liquid Multiphase Systems” (subproject B1). Financial support by the Deutsche Forschungsgemeinschaft (DFG, German Research Foundation) is gratefully acknowledged (SFB-TR 63).

Furthermore, the authors would like to thank their student Marina Goedecke for her help during the experiments.

References

- Baldi S, Yianneskis M (2003) On the Direct Measurement of Turbulence Energy Dissipation in Stirred Vessels with PIV *Industrial and Engineering Chemistry Research* 42:7006-7016
- Behr A, Roll R (2005) Hydroaminomethylation in thermomorphic solvent systems *Journal of Molecular Catalysis A: Chemical* 239:180-184
- Deen NG, Hjertager BH (2002) Particle image velocimetry measurements in an aerated stirred tank *Chemical Engineering Communications* 189:1208-1221 doi:10.1080/00986440213881
- Deen NG, Solberg T, Hjertager BH (2002) Flow generated by an aerated Rushton impeller: Two-phase PIV experiments and numerical simulations *Canadian Journal of Chemical Engineering* 80:638-652
- Dreimann JM, Warmeling H, Weimann JN, Künnemann K, Behr A, Vorholt AJ (2016) Increasing selectivity of the hydroformylation in a miniplant: Catalyst, solvent, and olefin recycle in two loops *AIChE Journal* doi:10.1002/aic.15345
- Hall JF, Barigou M, Simmons MJH, Stitt EH (2005) A PIV study of hydrodynamics in gas-liquid high throughput experimentation (HTE) reactors with eccentric impeller configurations *Chemical Engineering Science* 60:6403-6413 doi:10.1016/j.ces.2005.03.044
- Hentschel B, Kiedorf G, Gerlach M, Hamel C, Seidel-Morgenstern A, Freund H, Sundmacher K (2015) Model-Based Identification and Experimental Validation of the Optimal Reaction Route for the Hydroformylation of 1-Dodecene *Industrial & Engineering Chemistry Research* 54:1755-1765
- Kaiser NM, Flassig RJ, Sundmacher K (2016) Probabilistic reactor design in the framework of elementary process functions *Computers and Chemical Engineering* 94:45-59 doi:10.1016/j.compchemeng.2016.06.008
- Kämper A, Warrelmann SJ, Reischich K, Kuhlmann R, Franke R, Behr A (2016) First iridium-catalyzed hydroformylation in a continuously operated miniplant *Chemical Engineering Science* 144:364-371 doi:10.1016/j.ces.2016.01.054
- Kilander J, Rasmuson A (2005) Energy dissipation and macro instabilities in a stirred square tank investigated using an le PIV approach and LDA measurements *Chemical Engineering Science* 60:6844-6856 doi:10.1016/j.ces.2005.02.076
- Kim KC, Jeong EH, Kim SK, Adrian RJ (2001) A Study on the Turbulent Mixing Characteristics in a Rushton Turbine Reactor by PIV and PLIF *DLR-Mitteilung*:163-173
- McBride K, Gaide T, Vorholt A, Behr A, Sundmacher K (2016) Thermomorphic solvent selection for homogeneous catalyst recovery based on COSMO-RS *Chemical Engineering and Processing: Process Intensification* 99:97-106 doi:10.1016/j.cep.2015.07.004

- Montante G, Magelli F, Paglianti A (2013) Fluid-dynamics characteristics of a vortex-ingesting stirred tank for biohydrogen production *Chemical Engineering Research and Design* 91:2198-2208
doi:10.1016/j.cherd.2013.04.008
- Pan C, Min J, Liu X, Gao Z (2008) Investigation of Fluid Flow in a Dual Rushton Impeller Stirred Tank Using Particle Image Velocimetry *Chinese Journal of Chemical Engineering* 16:693-699
doi:10.1016/S1004-9541(08)60142-1
- Sharp KV, Adrian RJ (2001) PIV Study of small-scale flow structure around a Rushton turbine *AIChE Journal* 47:766-778
doi:10.1002/aic.690470403
- Sharp KV, Kim KC, Adrian RJ (1999) A comparison of dissipation estimation methods in a stirred tank using Particle Image Velocimetry (PIV) *Proceedings of the 1999 3rd ASME/JSME Joint Fluids Engineering Conference, FEDSM'99, San Francisco, California, USA, 18-23 July 1999 (CD-ROM):1*
- Sheng J, Meng H, Fow RO (2000) A large eddy PIV method for turbulence dissipation rate estimation *Chemical Engineering Science* 55:4423-4434
- Sheng J, Meng H, Fox RO (1998) Validation of CFD simulations of a stirred tank using particle image velocimetry data *Canadian Journal of Chemical Engineering* 76:611-625
- Sudiyo R, Virdung T, Andersson B (2003) Important factors in bubble coalescence modeling in stirred tank reactors *Canadian Journal of Chemical Engineering* 81:557-565
- Wieneke B (2015) PIV uncertainty quantification from correlation statistics *Measurement Science and Technology* 26:074002
- Yoon HS, Hill DF, Balachandar S, Adrian RJ, Ha MY (2005) Reynolds number scaling of flow in a Rushton turbine stirred tank. Part I - Mean flow, circular jet and tip vortex scaling *Chemical Engineering Science* 60:3169-3183 doi:10.1016/j.ces.2004.12.039
- Yoon HS, Sharp KV, Hill DF, Adrian RJ, Balachandar S, Ha MY, Kar K (2001) Integrated experimental and computational approach to simulation of flow in a stirred tank *Chemical Engineering Science* 56:6635-6649
doi:10.1016/S0009-2509(01)00315-3
- Zagajewski M, Behr A, Sasse P, Wittmann J (2014) Continuously operated miniplant for the rhodium catalyzed hydroformylation of 1-dodecene in a thermomorphic multicomponent solvent system (TMS) *Chemical Engineering Science* 115:88-94 doi:10.1016/j.ces.2013.09.033
- Zagajewski M, Dreimann J, Thönes M, Behr A (2016) Rhodium catalyzed hydroformylation of 1-dodecene using an advanced solvent system: Towards highly efficient catalyst recycling *Chemical Engineering and Processing: Process Intensification* 99:115-123
doi:10.1016/j.cep.2015.06.014
- Zlokarnik M (2001) *Stirring : theory and practice*. Wiley-VCH, Weinheim



Figure 1 Principle of thermomorphic solvent system (top) according to (Behr and Roll 2005). Pictures of the corresponding states in the reactor used for the present study (bottom); left: two-phase state at lower temperature ($T < 85\text{ °C}$); right: single-phase state at higher temperature, $T > 90\text{ °C}$ (stirrer shaft, temperature probe and gas tube are visible inside the reactor for the single-phase state).

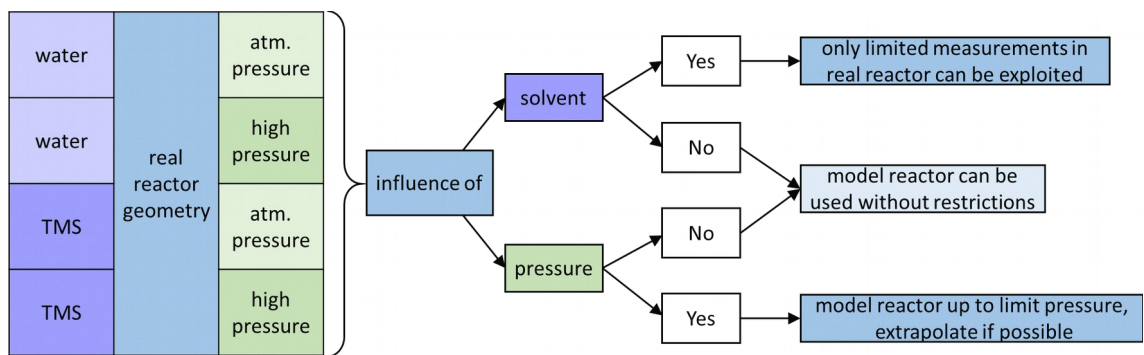


Figure 2 Measurement strategy

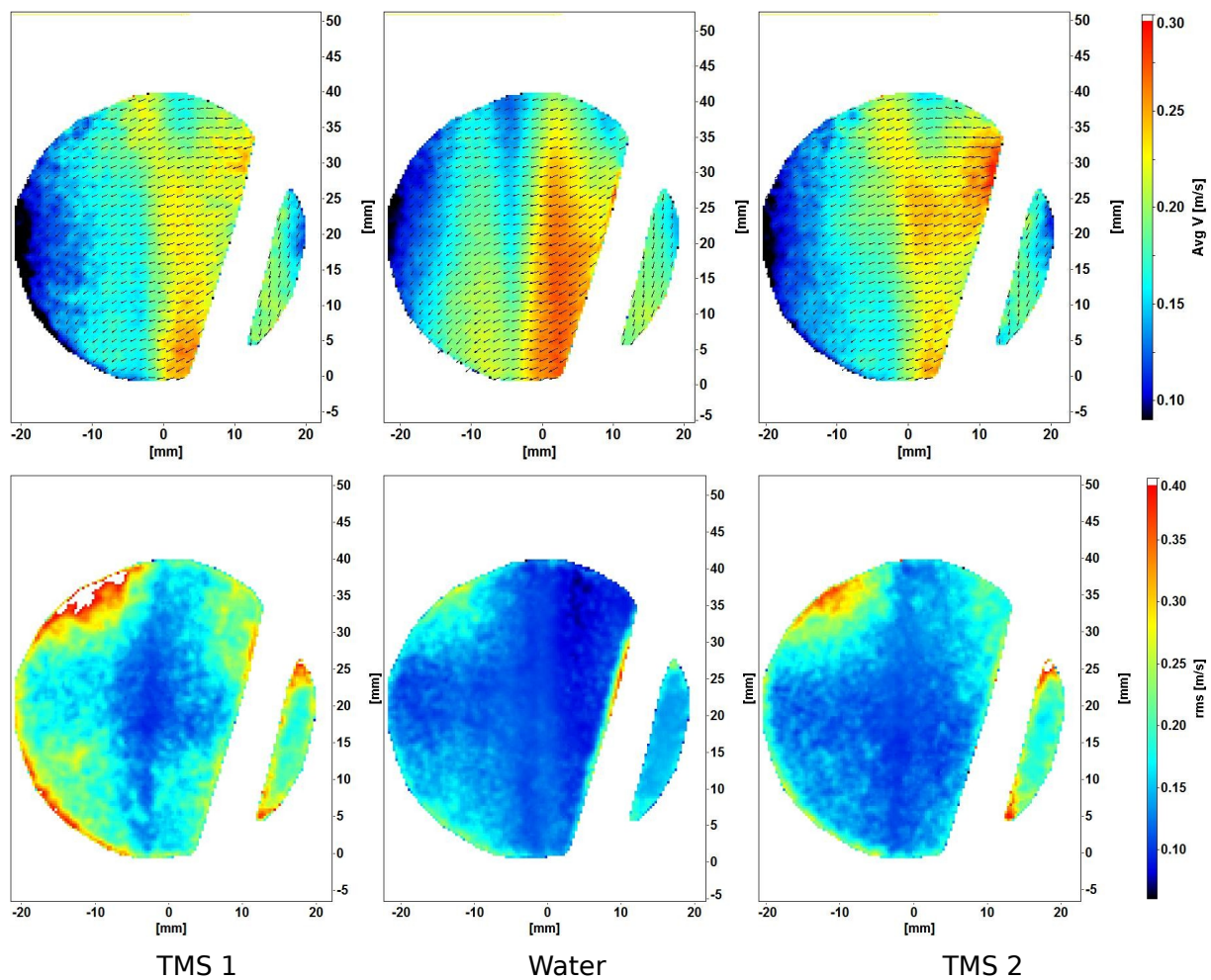


Figure 4 Averaged velocity magnitude (top) and standard deviation of magnitude (bottom) in different solvents at 5bar and 400rpm in m/s.

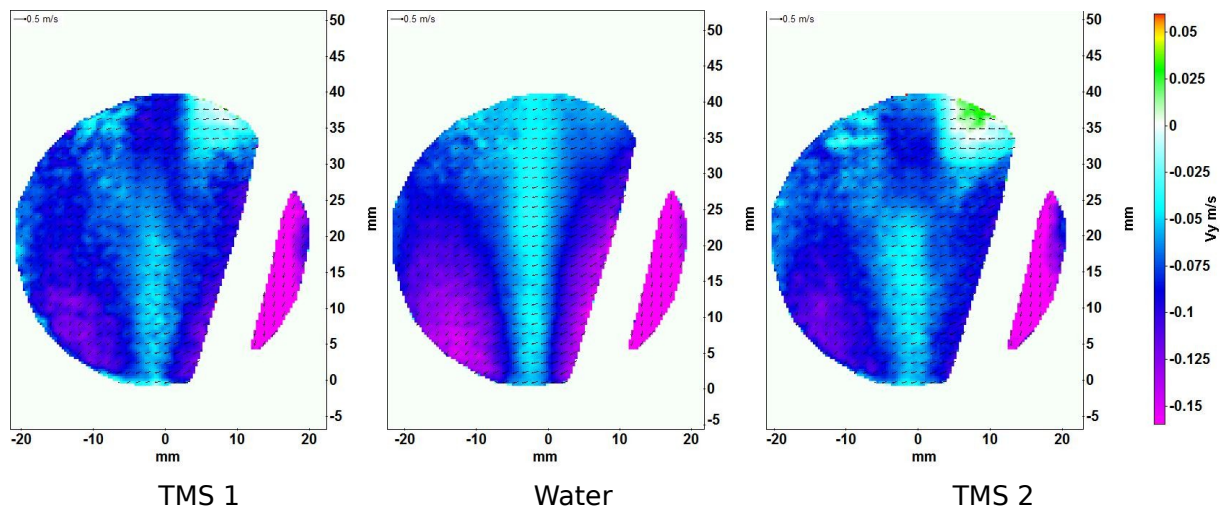


Figure 5 Vertical velocity component v_y in different solvents at 5bar and 400rpm in m/s.

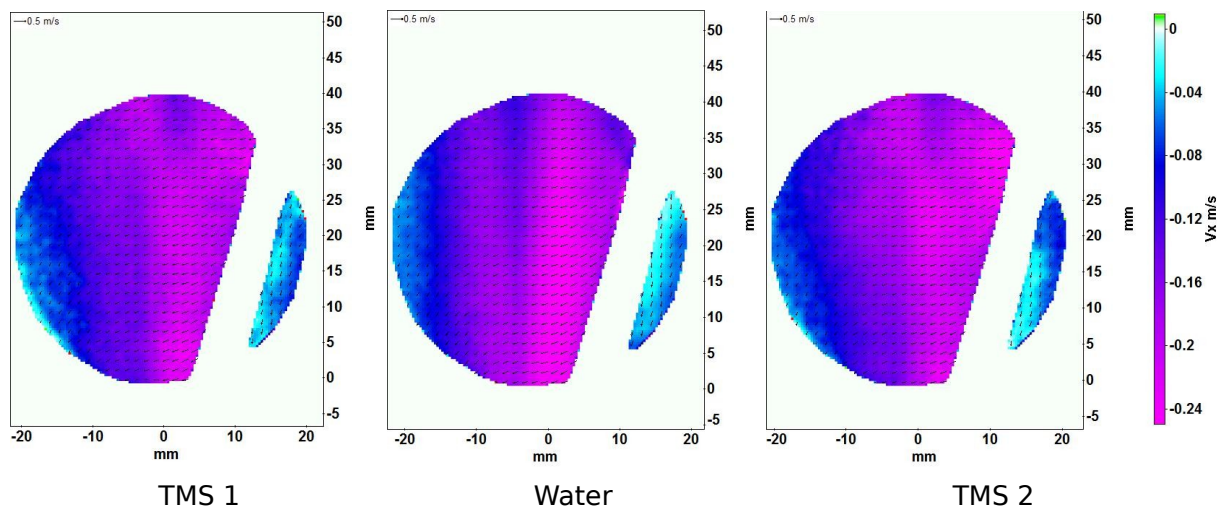


Figure 6 Horizontal velocity component v_x in different solvents at 5bar and 400rpm in m/s.

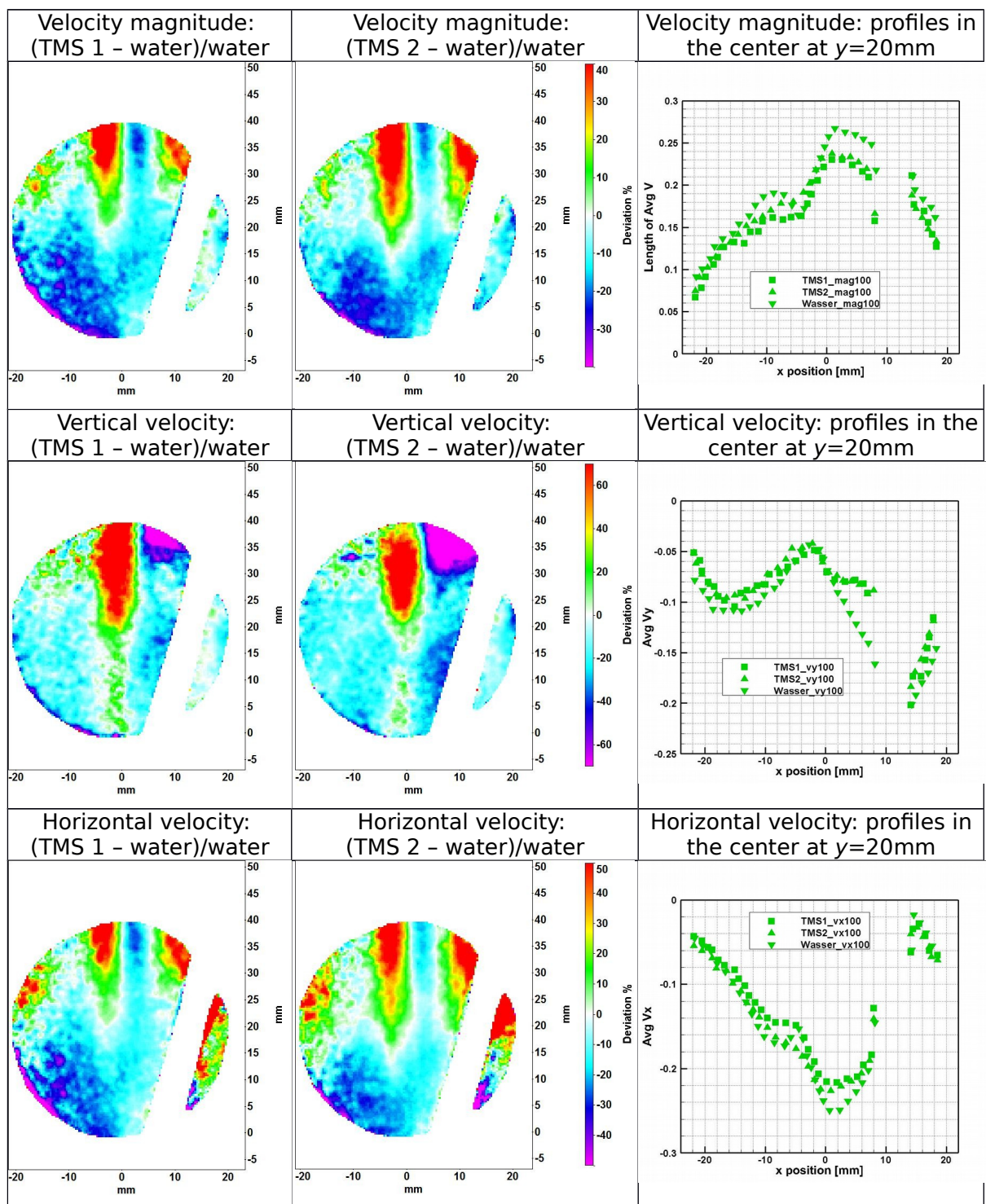


Figure 7 Relative mean velocity differences between water and TMS solvent systems in % at 5bar and 400rpm. Left: TMS1; centre: TMS2; right: absolute velocity profiles in the centre of the window at y=20mm. Top: mean velocity magnitude; centre: mean vertical velocity component; bottom: mean horizontal velocity component.

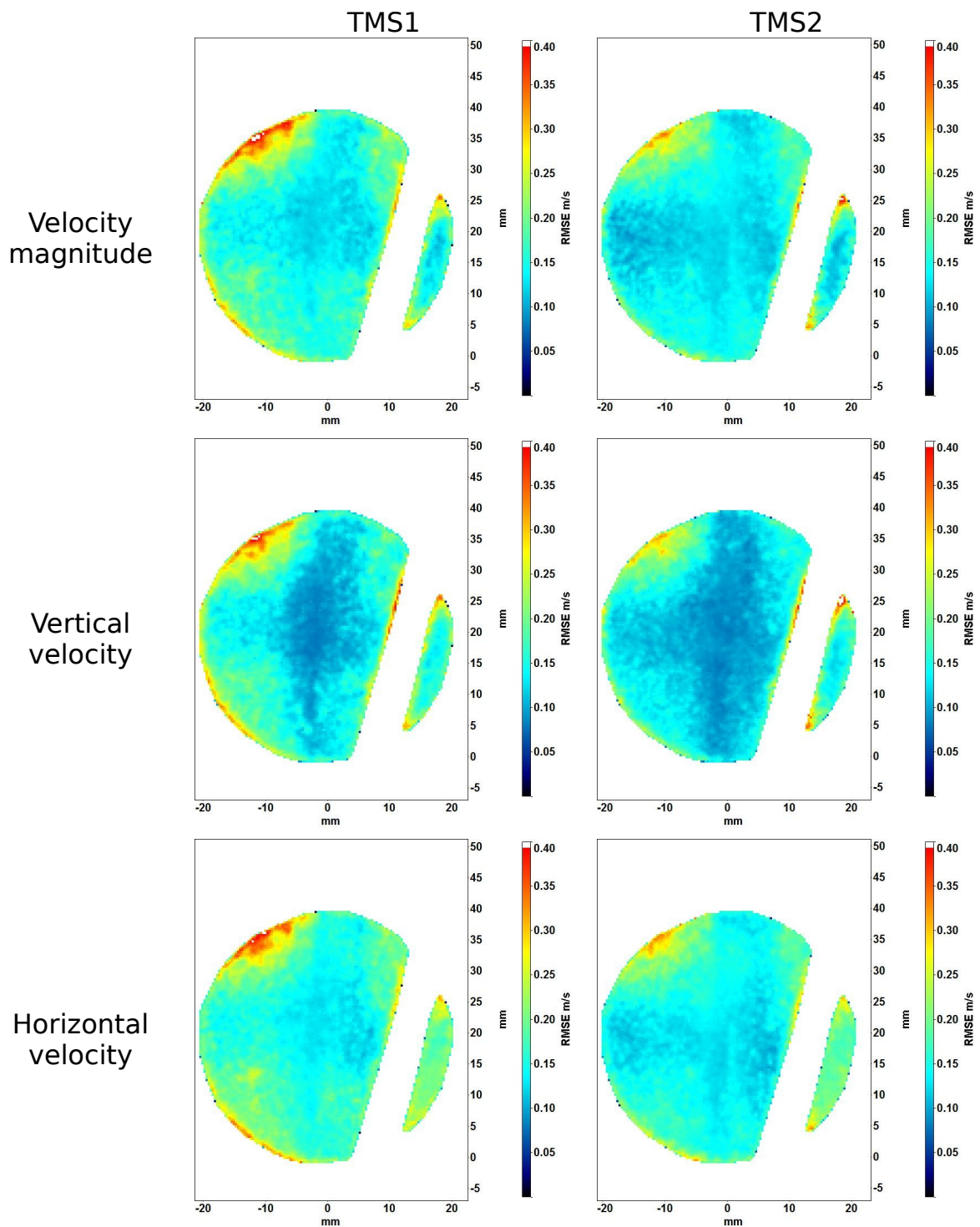
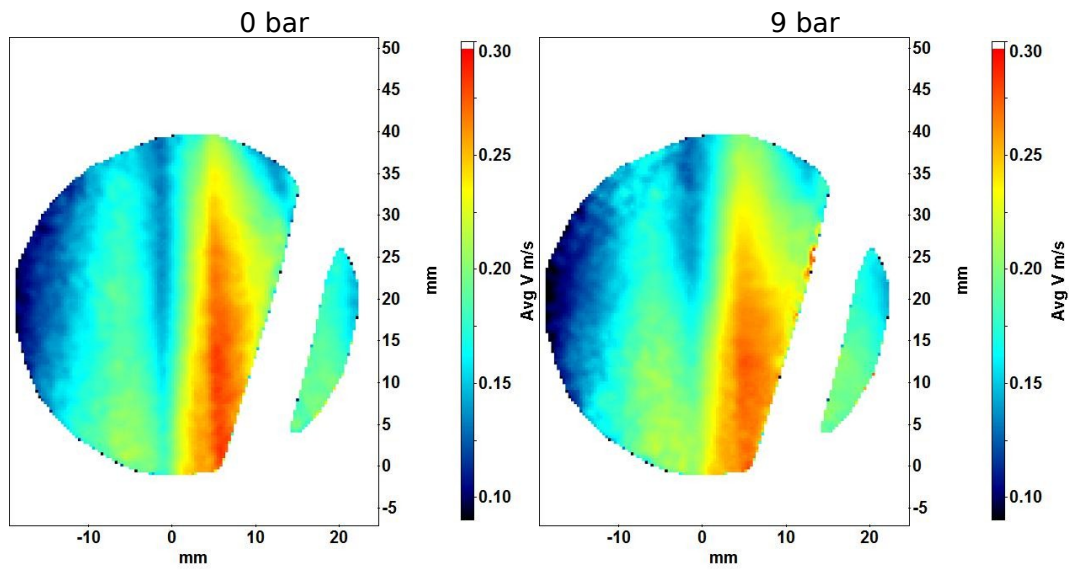


Figure 8 Root-mean square difference between TMS solvent systems and water of velocity magnitude (top), vertical velocity component (centre) and horizontal component (bottom) in m/s at 5 bar and 400 rpm. Left: TMS1; right: TMS2.



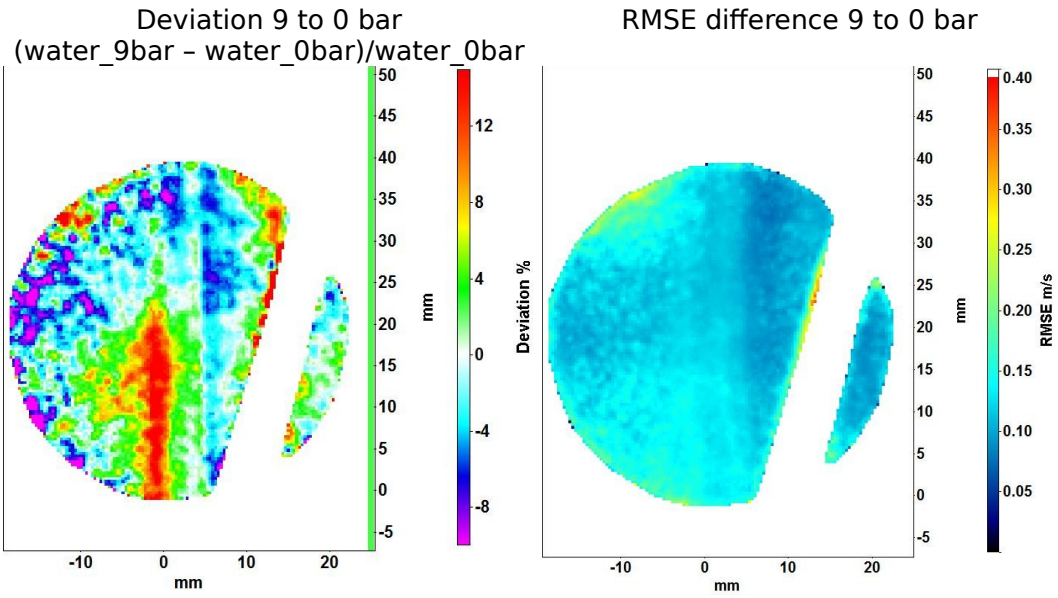


Figure 9 Averaged velocity magnitude [m/s] in water for 0 and 9 bar at 400rpm (top) and relative mean deviation in % (bottom, left) and RMSE difference (bottom, right).

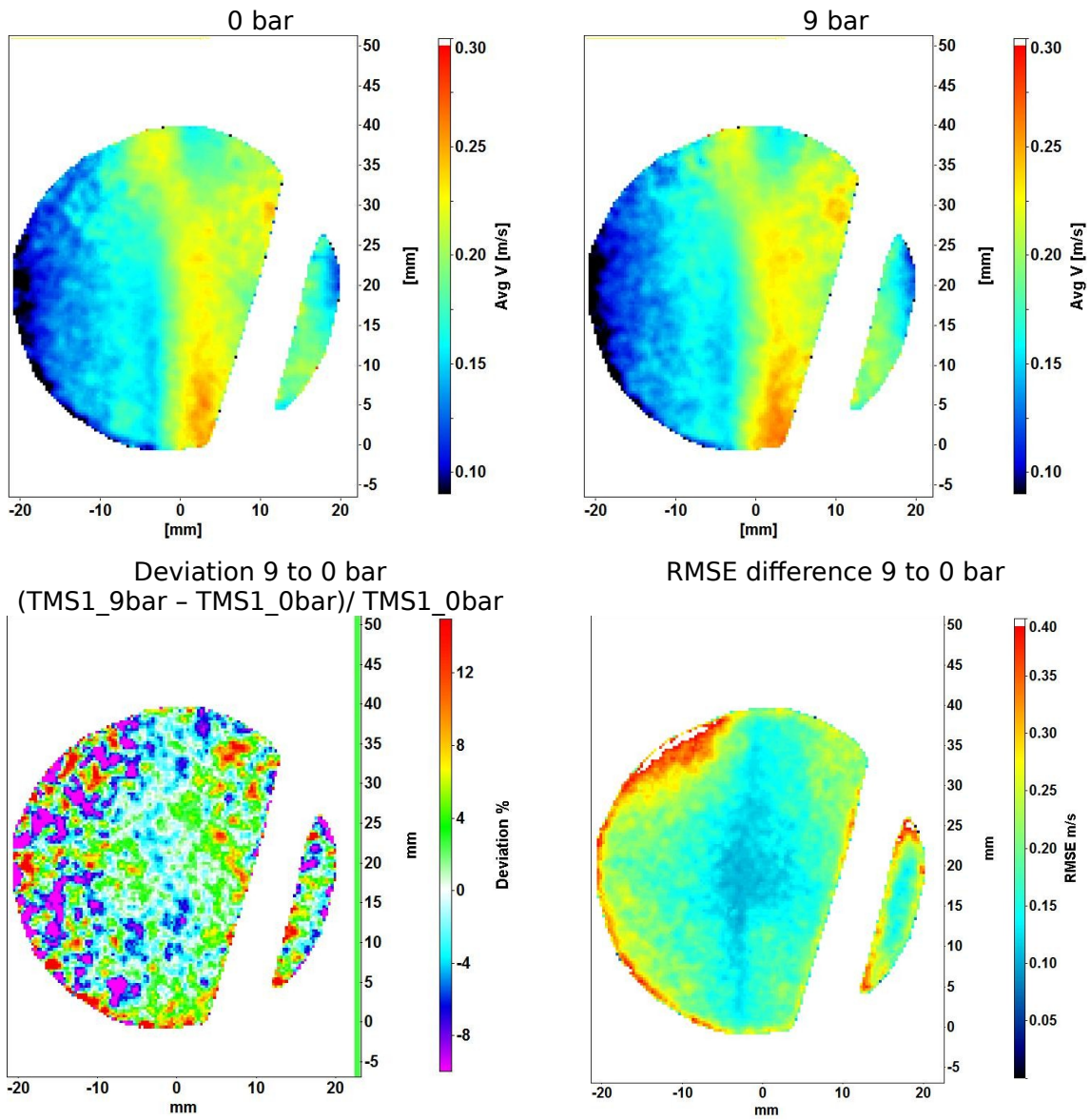


Figure 10 Averaged velocity magnitude [m/s] in TMS1 for 0 and 9 bar at 400rpm (top) and relative mean deviation in % (bottom, left) and RMSE difference (bottom, right).

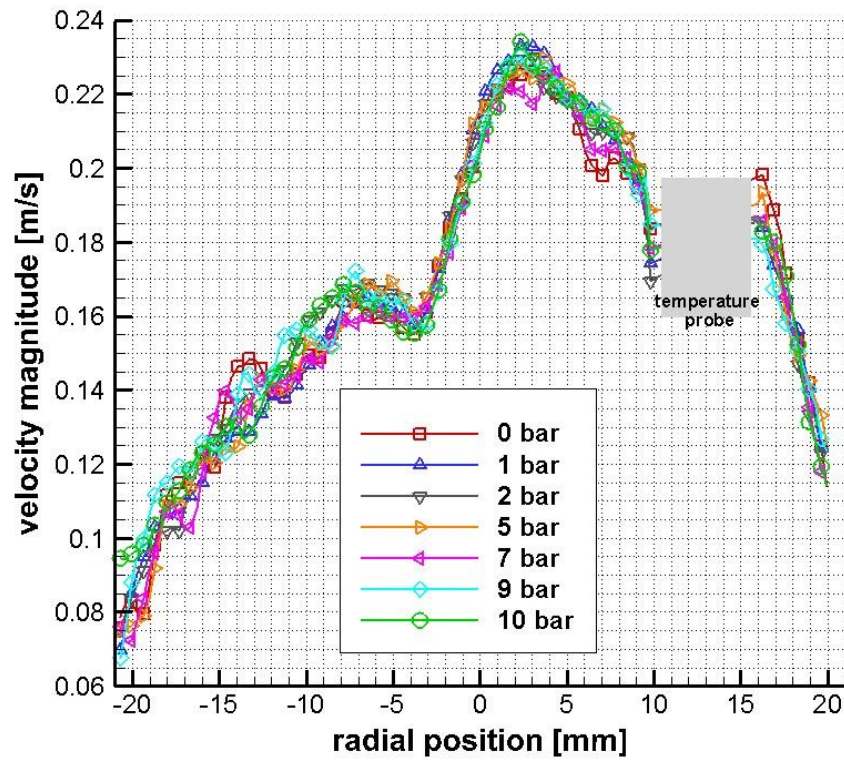


Figure 11 Averaged velocity magnitude profiles (m/s) in TMS1 at 400rpm for different pressure in the centre position of the window ($y=20\text{mm}$).